Supporting Information

Ormond and McNaughton 10.1073/pnas.1421963112

SI Experimental Procedures

Animals and Surgery.

Chronic recording. Six male Fisher–Brown Norway hybrid rats (300–400 g; 8–14 mo old) were implanted with unilateral ($n = 3$) or bilateral ($n = 3$) cannulae targeting between one to three sites along the dorsoventral axis of the MEC (see Fig. 1 for location of sites). In five of six animals, cannulae reached the superficial layers of MEC. In the sixth, the cannulae were slightly off target in the deep layers of intermediate MEC; given that muscimol would likely have diffused to the superficial layers (and likewise, superficial injections likely spread to some degree to the deep layers), we chose to include the data from this animal. Implant coordinates for the cannulae were centered at between 4.5 mm lateral of midline and 0.2 mm anterior to the transverse sinus for dorsal sites to 5.0 mm lateral of midline and 0.5 mm anterior to the transverse sinus for ventral sites. During the same surgery, animals were implanted with a custom-designed recording array containing 18 drivable tetrodes and 3 drivable single-channel electrodes (tetrodes with only one channel connected to the recording system; see below for details). The three bundles were implanted over the hippocampus from 2 mm posterior to bregma and 1 mm lateral to midline to 5 mm posterior to bregma and 4.5 mm lateral to midline. Recording electrodes were turned down to targets in the hippocampus over the course of 2–4 wk. Electrodes were usually turned to CA1 first, and after sufficient data had been collected there, they were turned down to CA3 over the course of another week. One single-channel electrode was turned to corpus callosum and served as a reference which was subtracted from all other recording channels. The other two single-channel electrodes were turned to the hippocampal fissure to record the theta rhythm; only data from the electrode that detected the greatest theta power during the baseline period for a given day was used in subsequent analysis. At the end of the physiological recordings, a small anodal DC current (5–10 μA, 10 s) was applied to the recording sites ∼7 d before the animals were perfused. The rats were deeply anesthetized with a lethal dose of pentobarbital and perfused first with chilled PBS, and then chilled 4% (wt/vol) paraformaldehyde in PBS. The positions of the electrodes and cannulae were confirmed histologically using a cresyl violet-staining procedure. One stainless-steel screw inserted above the cerebellum served as the ground electrode during recordings. All protocols were approved by the Animal Welfare Committee of the University of Lethbridge.

Anesthetized recording. To assess the spread of muscimol from entorhinal injection sites, studies were conducted in anesthetized rats while recording simultaneously at several sites in MEC. Six Long Evans rats (400–450 g; 3–4 mo old) were anesthetized with urethane (initial i.p. injection of 3 mL of 20% urethane in PBS, supplemented with 0.2-mL injections as needed; final dose, 1.2–1.4 g/kg). Craniotomies were made over left and right MEC. An array containing four tetrodes and a cannula guide with injector cannula inserted were lowered into the right MEC; the injector tip was either level with the tetrode tips (distance between injector and tetrodes, ∼0.5 mm) or protruded 2 or 4 mm below the tetrodes. The electrodes were slowly lowered until spiking activity was observed on at least one tetrode. After a baseline recording period, 0.4 μL of muscimol (8.8 mmol in PBS) was infused at a rate of 0.1 μL/min; recording continued for 30 min. The recording/infusion procedure was then repeated in the left hemisphere.

Behavioral Training. Animals were pretrained in the running task. The horseshoe track is a circular track with a barrier at one point. The rat runs from one side of the barrier to the other, consumes food reward, and then turns around and runs back to the side of the barrier from which he started and again consumes food reward; this sequence comprises one clockwise lap and one counterclockwise lap. Animals were food deprived down to not less than 85% of their ad libitum body weight. Their feed was switched from solely laboratory feed pellets, to laboratory feed pellets soaked into a mash and mixed with apple sauce. They received food in the reward wells during track running and initially also in the home cage; mash was delivered manually by the experimenter. Over the course of training, the amount of food deposited in the reward wells was reduced to minimize electrical chewing artifacts, but at the end of sessions the remainder of the food was dispensed in a small number of laps (not used for analysis), with no food being offered in the home cage; this system of feeding appeared to produce optimal behavior for the task. After reaching criterion (∼15–20 runs in each direction), animals were taken off food deprivation, and surgically implanted. After a 1-wk recovery period, training recommenced, always necessary to ensure adequate behavior by the time electrodes reached their targets.

Behavioral Testing and Infusions. A typical recording session began with a minimum 15-min rest period in a towel-lined pot in the center of the track, followed by a baseline running session consisting of 10–25 runs in each direction (always the same number of laps for trials on a single day). While still plugged into the recording system, the rat was wrapped in a towel in such a way that only the top of the recording array, from which the cannulae emerge, was exposed to the experimenter. The stylet was removed from the cannula, and an injector was inserted. Injectors were attached to Hamilton syringes loaded in a Harvard Apparatus syringe pump by way of PE20 tubing, filled with water; movement of a small bubble near the connection to the injector, as well as a postinjection verification that the injector was not clogged, was used to confirm successful injection. Infusions were made at a rate 0.1 μL/min, and once complete, the injector was left in place for 4 min. The next trial resumed ∼5 min after the end of the infusion. In some sessions, multiple infusions were made as follows: if the previous infusion was vehicle, a second muscimol infusion of low or high concentration could be made following the subsequent running trial; if the previous infusion was low-concentration muscimol, a high-concentration muscimol infusion was sometimes made following the subsequent running trial. Thus, in a single session, a maximum of three infusions and four running trials was possible.

Animals required 5–15 min to complete each trial. Each rat seemed to have a slightly different level of motivation, and each rat's level of motivation could change across days, typically as they got accustomed to being in a food-deprived state. Generally, the experimenter would decide the number of laps per trial based on the amount of motivation the animal had displayed the previous day—i.e., if the animal seemed less motivated, then fewer laps would be run per trial so that all trials could be completed before the animal started showing reduced running speeds or unwillingness to keep running.

Cannula guides were constructed from 25-gauge hypodermic tubing, typically with guides glued together into arrays of two or three. Guides were ∼50 mm long, as they had to enter a hole in the bottom of the electrode array, coming up through the protective cone and ending just above the level of the electrode interface board. This configuration was necessary to allow both the cannulae and electrode array to fit on the skull, given the

close proximity of the hippocampus and MEC. Injectors were constructed from 32-gauge hypodermic tubing and, when inserted into the guide, protruded by between 1 and 5 mm into the brain.

We used muscimol (Tocris; five rats) or muscimol hydrobromide (Sigma; one rat) for inactivations. The drug was dissolved in PBS to a final concentration of between 2.2 and 2.6 mM for low-concentration doses, and between 8.8 and 10.3 mM for high-concentration doses (muscimol hydrobromide was used at the higher concentrations to account for its presumably more limited diffusion due to its higher molecular weight), except in one rat that was not able perform the task after a high-concentration dose; this rat instead had a high concentration of 4.4 mM. The volume of injections was between 0.4 μL (five rats) and 0.5 μL (one rat). Three rats received bilateral infusions, and four rats received unilateral infusions (one rat received both). Most unilateral infusions were to intermediate and ventral sites (except for one rat which received low-concentration dorsal infusions unilaterally); we observed no differences between the unilateral and bilateral treatments, consistent with the weak contralateral projection originating mainly from dorsal MEC in the rat (1, 2).

Electrode Array Design. We designed our electrode array based on the design by Kloosterman and colleagues (3). Using Solidworks software, we modified their design to accommodate three recording bundles running along the dorsoventral axis of the dorsal half of the hippocampus (bundle 1, dorsal; bundle 2, dorsal-intermediate; bundle 3, intermediate). We also designed cuts through the protective cone and array to allow long cannulae implanted in the MEC to slide up and into the drive during implantation (Fig. 1).

Data Collection. Tetrodes consisted of four polyimide-coated, nichrome wires (14-μm diameter) twisted together, and with tips gold-plated to impedances ranging from 0.1 to 0.4 MΩ [see Nguyen et al. (3) for a video of the process] in the presence of polyethylene glycol to reduce short circuits between the individual channels (4). Neural signals were recorded using a Neuralynx digital Cheetah system. Signals were filtered between 2 and 500 Hz, had a reference signal from corpus callosum subtracted, and were then sampled at ∼32 kHz for spike channels or ∼2 kHz for local field potential (LFP) channels. Animal position was tracked using reflective red and blue tape (3M) along with white LEDs and a video camera positioned on the ceiling; position was determined by crossing of the red and blue light thresholds set in the Cheetah software. Spike threshold was set at 50 μV for all spike channels, and a file containing spike waveforms and time stamps for each tetrode was generated.

Analysis. All analysis was performed in Matlab.

Analysis of theta power. Theta power was calculated from single electrodes located in the hippocampal fissure using the mtspecgramc function (for multitaper time-frequency spectrum–continuous process) available in the Chronux open-source software package (5). LFP data were restricted to the same running epochs as spike data (see below), then concatenated into a single vector, and analyzed using a window size of 5 s, with successive windows shifted in 2.5-s increments. Theta frequency and peak power were determined by finding the peak of the power spectrum between 6 and 10 Hz. Second harmonic frequency and peak power were determined by finding the peak of the power spectrum between 13.5 and 18.5 Hz. Sessions with peak theta power less than 0.03 mV^2 during the baseline period were discarded from the analysis; note that this cut-off value does not reflect the true power of the signal as the tapers reduce the amplitude of the signal from which the power is calculated.

Spike sorting, identification of place cells, and restriction of spike data. Spikes from each tetrode file were automatically clustered into ∼30 clusters using KlustaKwik (K. D. Harris, University College of London, London; http://klustakwik.sourceforge.net/). These clusters were then loaded into custom-written software (Drifter; K. Godfrey, Allen Institute for Brain Science, Seattle) that plotted the track position of all spikes for each cluster during the baseline period, as well as the firing rate over time for both baseline and treatment periods. Generally for a given cluster, if no spikes were fired on the track during the baseline period and no increase in firing rate was seen during the treatment period, and if it had no overlap with another cluster with these properties, then the cluster was discarded. Remaining clusters were merged and/or split as appropriate, using cross-correlations and comparisons of spike amplitude, energy, and principal components across tetrode channels (6). Clusters with more than 0.5% of spikes fired in the first 2 ms of the autocorrelation or that were not well separated from all other spikes in at least one projection in cluster space were discarded from analysis. Interneurons were identified on the basis of spike shape, width, shape of the autocorrelation (principal cell autocorrelations tend to peak immediately after the absolute refractory period, whereas interneuron autocorrelations tend to peak with a delay), as well as the fact that the vast majority tended to fire spikes over the entire track.

Only epochs longer than 1 s when the rat was moving with a velocity greater than 5 cm/s were included in the analysis. Data were further restricted around the reward wells (where head movement could potentially reach velocity threshold) as follows: the track was linearized by converting angular position to a linear position, and split into 200 bins; occupancy was plotted separately for baseline and treatment trials; clear peaks were seen in the plotted occupancy at the reward wells due to relatively lower velocities as the animal left or approached the wells; the bins over which the animal ran were bounded by the first and second peak for the counterclockwise run and the third and fourth peak for the clockwise run. Data from bins outside these two areas of the track were discarded. Spatial information (7) and firing rate were then calculated for remaining units. Units whose spatial information score did not reach 0.4 or whose maximum firing rate did not reach 1 Hz in either the baseline or treatment trial were discarded from the analysis. This left a total of 518 place cells in CA1 and 351 place cells in CA3.

Firing-rate population vector analysis. For the firing-rate population vector analysis (8, 9), binned firing rates were calculated for each unit by dividing the total number of spikes fired at a given track bin by the occupancy at that bin. The firing rates of all units at a single bin were then combined into a population vector. The dot product could then be calculated between pairs of bins; a value of 1 indicates perfect correlation (i.e., the relative magnitudes of the firing rates is identical, although the absolute magnitudes may be different), whereas a value of 0 indicates no correlation (i.e., completely orthogonal vectors). After calculating dot products for all pairs of vectors, a heat map of the dot product values was made by plotting each value at the x and y positions corresponding to the identities of vector 1 and vector 2 (Fig. 3*B*). The width of the area of high heat running along the diagonal from lower left to upper right gives an indication of the scale of the spatial representation. This can be quantified by constructing a curve from the interval in track bins between each pair of vectors and their corresponding correlation value (Fig. 3*C*). The distance in bins at which the average correlation drops to 0.5 could then be easily calculated from the curve. In a small number of cases, the correlation value after inactivation never dropped to 0.5; in these cases, the target correlation value was increased by 0.1 increments until a valid value was found.

Individual field analysis. To identify individual place fields, we defined place fields as being composed of spikes fired at a specific location in the environment displaying phase precession relative to the theta rhythm recorded in the hippocampal fissure. LFP recorded in the fissure was filtered for theta [bandpassed between

6–10 Hz; eegfilter from the EEGLAB open source software package (10)] and theta phase for each sample calculated using the Hilbert function. Because the LFP was sampled at a lower frequency than spikes, spike times fell between adjacent LFP samples; thus, theta phase of individual spikes was interpolated using the built-in interp1 function. A script was written to randomly select a unit from either the baseline or treatment period, and display the phase and position information for its spikes. The experimenter could then select boundaries around place fields without knowledge of the tetrode or trial from which the data originated. Fig. 4*B* shows an example of the display, with fields color-coded to demonstrate the selections made by the experimenter. First, any fields which overlapped other fields were discarded, such as the first two small fields on the far left. Second, any fields that overlapped the reward areas (gray boxes) were excluded because these fields may have been truncated; the blue field is an example of this. Finally, what remained were place fields that did not overlap either other fields or reward areas, such as the red field. Relative position and theta phase of all spikes from selected place fields could then be plotted in a single heat map to verify that boundaries were selected consistently across the two trials (i.e., fields were not either consistently truncated, which would show incomplete precession, or arbitrarily expanded, which would show large blank areas at the beginning and ends of the plots; Fig. 4*C*). The boundaries of these fields were then used to calculate the width of the place fields.

We used the place field boundaries from this analysis to separate the rate maps used in the firing-rate population vector analysis into in-field and out-of-field rate maps for each place cell (Fig. S7 *A*–*C*). Infusion trial in-field and out-of field rate maps were then adjusted so that their mean rates equaled those for baseline trials; this was done by multiplying the infusion trial in-field rate map by the baseline trial mean in-field rate divided by the infusion trial mean in-field rate for each place cell, and likewise for out-of-field rate maps. Subsequently, the in-field and out-of-field rate maps for each cell were combined to make a complete rate map spanning the track, and the firing-rate population vector analysis was performed with these new rate maps, providing a control for the effect of changing in-field and out-of-field rates after infusions (Fig. S4 *B*–*D*).

Remapping analysis. To assess remapping, two analyses were performed. In the first, Pearson correlation coefficients were calculated for pairs of population vectors (same population vectors as the firing-rate population vector analysis in Fig. 3) from the same track bin before and after vehicle or muscimol infusion. In the second, Pearson correlation coefficients were calculated between pairs of rate maps for each individual unit (the same units as included in the firing-rate population vector analysis in Fig. 3) before and after vehicle or muscimol infusion.

Paired field analysis. For the paired field analysis (Fig. 5), the place fields were further restricted to fields that could be identified as being present during both baseline and treatment trials. A center of mass was calculated for each previously selected field by calculating the mean position of all spikes. Fields from the baseline and treatment trials that bounded each other's centers of mass were then paired for subsequent analysis.

The phase precession slope was calculated using the circular regression method of Kempter et al. (11). This method uses an iterative algorithm; in a small number of cases when phase precession was relatively weak, the phase value converged to zero, in which case the data were discarded from the analysis.

To calculate autocorrelograms for each paired place field, the intervals between each spike and all subsequent spikes within a 2-s window were calculated and plotted as a histogram (only the first second is displayed; Fig. 5*B*). The autocorrelation was concatenated to the end of a mirror image of itself to avoid boundary issues, and theta power was calculated as for the LFP. Intrinsic oscillation frequency was calculated as the peak power between 6 and 12 Hz. Data were restricted to autocorrelations with a minimum of four counts in the peak bin. Theta modulation was calculated by filtering the autocorrelogram for theta (between 6 and 12 Hz) and subtracting the value of the first trough from the average of the first two peaks and dividing the total by the average of the first two peaks; if the trough value reaches 0, the score is 1, indicating strong theta modulation, if the trough value equals the average value of the first two peak values, the score is 0, indicating no theta modulation; data was further restricted to fields that had a theta modulation value greater than 0.35.

Lap-by-lap paired place field analysis. For the lap-by-lap analysis of place field scale (Fig. 6), spikes from paired fields were assigned to individual laps for each trial. Place field width for each lap was then calculated by subtracting the position of the final spike for that lap from the first spike. To verify this analysis using a method that did not rely on manually selected phase precession boundaries, we developed a method that used a firing-rate threshold and binned firing rates. For each paired place field, binned rate maps for the corresponding place cell were constructed for each lap. The algorithm then searched for bins over a firing rate of 0.5 Hz, starting from the field center (calculated in the paired field analysis above). Because bins over threshold could be relatively sparse on a single lap, the algorithm tolerated gaps of up to five bins below threshold between bins over the threshold before completing the search. The field width was then calculated as the distance in bins between the first and last bin for each lap.

Statistics. All statistical analysis was performed in Sigmaplot. Bar graphed data are presented as mean ± SEM. For statistical analyses between pairs of treatments whose values were normally distributed (tested using the Shapiro–Wilk test) and had equal variance, we used t tests with significance set at $P < 0.05$. For analyses between pairs of treatments whose values were not normally distributed or did not have equal variance, we used the Mann–Whitney U test with significance set at $P < 0.05$. For the analysis of interneuron firing rates before and after infusions, we used paired t tests for treatments whose values were normally distributed, and Wilcoxon signed-rank tests for treatments whose values were not normally distributed, both with significance set at $P < 0.05$. For statistical analyses between multiple treatments whose values were normally distributed and had equal variance, one-way ANOVAs were used. If a significant difference was found between treatments ($P < 0.05$), post hoc multiple comparisons were performed using the Holm–Sidak method with a significance level of 0.05 to identify which inactivation treatments were different from vehicle control. For statistical analyses between multiple treatments whose values were not normally distributed or did not have equal variance, Kruskal–Wallis one-way ANOVA on ranks tests were performed. If a significant difference was found between treatments ($P < 0.05$), post hoc multiple comparisons were performed using Dunn's method to identify which inactivation treatments were different from vehicle control ($P < 0.05$). To identify differences among muscimol inactivation groups using infusion site as a factor, two-way ANOVAs were used. If a significant difference was found between treatments ($P < 0.05$), post hoc multiple comparisons were performed using the Tukey test.

Grid Cell Modeling. The model (Fig. S9 *B*–*D*) is a reproduction of the model published by Solstad et al. (12), incorporating the data on the number of grid modules and their spacing from Stensola et al. (13). Briefly, the changes to the Solstad model are that the number of grid modules is reduced to six [Stensola et al. (13) found five, but limited sampling of ventral MEC suggest the possibility of one or two additional grids with wider spacing]. The grid spacing ranged from 40 to 115 cm, with each grid having an internode spacing 1.4 times larger than the previous grid, again according to the findings of Stensola et al. (13). The weights of each grid were determined according to the formulas derived

from Fourier theory by Solstad et al. (12, 14). The threshold (or inhibition) was set empirically to produce a single field in the unlesioned condition; this level is approximately double that used in the original Solstad model, necessary due to the reduced number of input grids. In the reduced threshold condition, the threshold was reduced by 15%.

1. Goldowitz D, White WF, Steward O, Lynch G, Cotman C (1975) Anatomical evidence for a projection from the entorhinal cortex to the contralateral dentate gyrus of the rat. *Exp Neurol* 47(3):433–441.
2. Steward O (1976) Topographic organization of the projections from the entorhinal area to the hippocampal formation of the rat. *J Comp Neurol* 167(3):285–314.
3. Nguyen DP, et al. (2009) Micro-drive array for chronic in vivo recording: Tetrode assembly. *J Vis Exp* 2009(26):1098.
4. Ferguson JE, Boldt C, Redish AD (2009) Creating low-impedance tetrodes by electroplating with additives. *Sens Actuators A Phys* 156(2):388–393.
5. Bokil H, Andrews P, Kulkarni JE, Mehta S, Mitra PP (2010) Chronux: A platform for analyzing neural signals. *J Neurosci Methods* 192(1):146–151.
6. Harris KD, Henze DA, Csicsvari J, Hirase H, Buzsáki G (2000) Accuracy of tetrode spike separation as determined by simultaneous intracellular and extracellular measurements. *J Neurophysiol* 84(1):401–414.
7. Skaggs WE, McNaughton BL, Wilson MA, Barnes CA (1996) Theta phase precession in hippocampal neuronal populations and the compression of temporal sequences. *Hippocampus* 6(2):149–172.
8. Battaglia FP, Sutherland GR, McNaughton BL (2004) Local sensory cues and place cell directionality: Additional evidence of prospective coding in the hippocampus. *J Neurosci* 24(19):4541–4550.
9. Maurer AP, Vanrhoads SR, Sutherland GR, Lipa P, McNaughton BL (2005) Self-motion and the origin of differential spatial scaling along the septo-temporal axis of the hippocampus. *Hippocampus* 15(7):841–852.
10. Delorme A, Makeig S (2004) EEGLAB: An open source toolbox for analysis of single-trial EEG dynamics including independent component analysis. *J Neurosci Methods* 134(1):9–21.
11. Kempter R, Leibold C, Buzsáki G, Diba K, Schmidt R (2012) Quantifying circular-linear associations: Hippocampal phase precession. *J Neurosci Methods* 207(1):113–124.
12. Solstad T, Moser EI, Einevoll GT (2006) From grid cells to place cells: A mathematical model. *Hippocampus* 16(12):1026–1031.
13. Stensola H, et al. (2012) The entorhinal grid map is discretized. *Nature* 492(7427):72–78.
14. Riley KFBS, Hobson MP (2006) *Mathematical Methods for Physics and Engineering* (Cambridge Univ Press, Cambridge, UK).

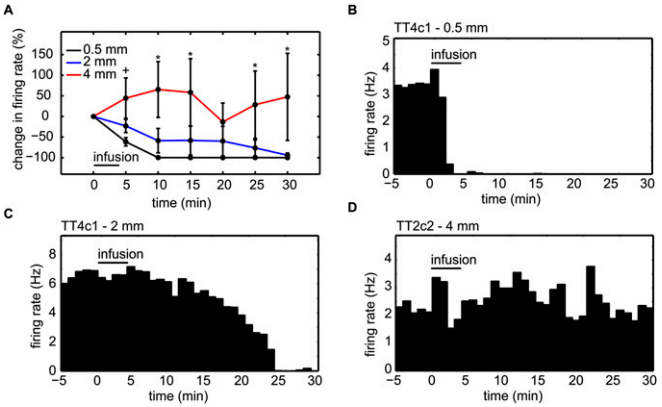

Fig. S1. Muscimol spread from infusion site after high-concentration infusion. There were no decreases in firing rates observed 4 mm from infusion site (approximate distance between dorsal and ventral infusion sites in behavioral experiments), but there were decreases at sites 2 mm away (approximate distance between intermediate and ventral/dorsal sites); the inactivation 2 mm from the infusion site was not complete until 25–30 min after the beginning of the infusion, by which point behavioral sessions were usually finished (*Experimental Procedures*). (*A*) Summary data, presented as mean ± SEM. Number of units recorded: 0.5 mm = 8; 2 mm = 10; 4 mm = 9. The plus sign (+) indicates significant difference between 4- and 0.5-mm groups, the single asterisk (*) indicates significant difference between 4- and 0.5-mm groups, and between 4- and 2-mm groups. (*B–D*) Example binned firing rates (1-min bins) before and after infusions for one cell from each group.

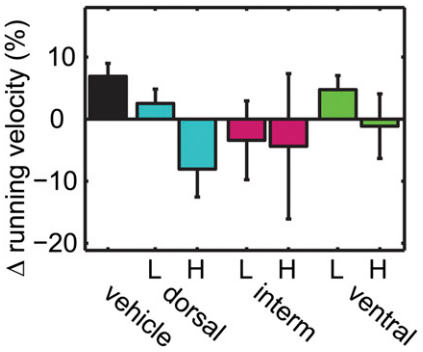

Fig. S2. Running velocity on the track after MEC infusions. Although there was a trend seen toward reduced running velocity after muscimol infusions compared with control, no significant differences were found. Muscimol treatments are subdivided into low (L)- and high (H)-concentration treatments. Vehicle or site of inactivation is listed along the *Bottom* (the intermediate treatment is abbreviated as "interm"). Data are presented as mean ± SEM. Ns: vehicle = 16; dorsal low = 7; dorsal high = 8; intermediate low = 6; intermediate high = 7; ventral low = 7; ventral high = 12.

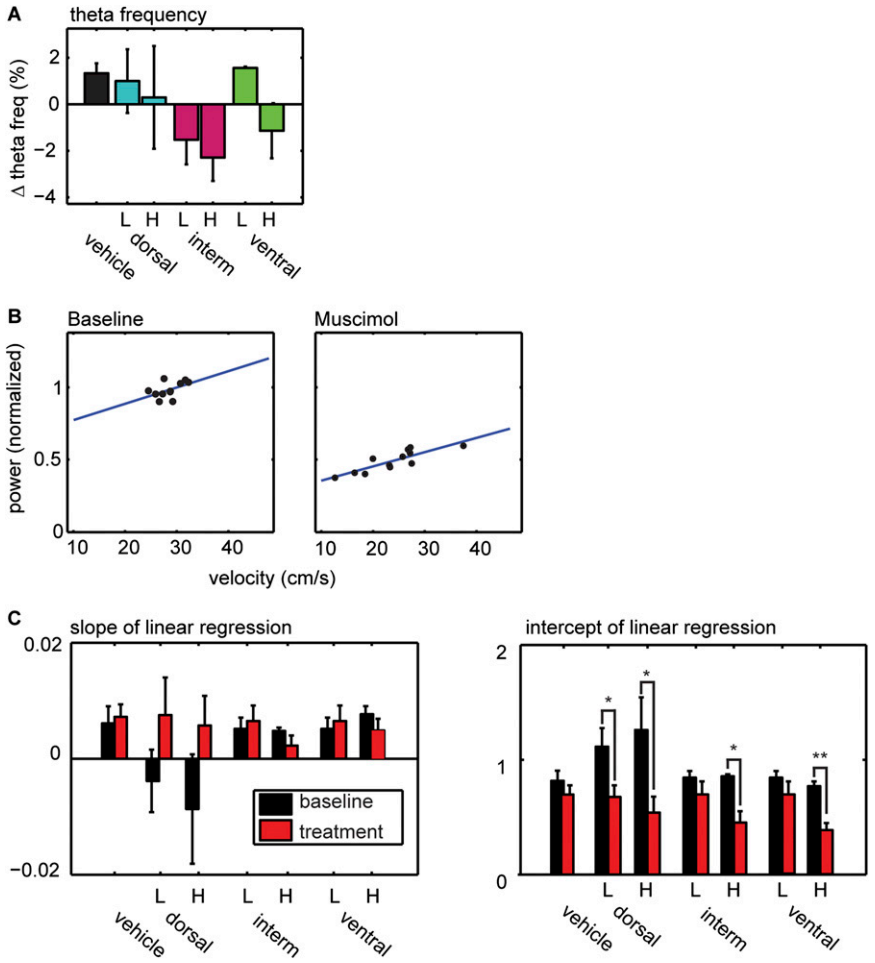

Fig. S3. Linear regression analysis of theta power vs. running velocity. The decrease in theta power after focal MEC inactivation was not due to nonsignificant decreases in running velocity, as there was a significant decrease in the *y* intercept of the linear regression in most inactivation treatments. (*A*) There were no significant changes in theta frequency after inactivations. (*B*) Representative linear regressions for one animal before and after high-concentration muscimol infusion to the ventral MEC. (*C*) Changes in slope of linear regression (*Left*) and *y* intercept of linear regression (*Right*) for each treatment. Theta power was normalized to the theta power at a velocity of 30 cm/s for the grouped analysis. Data are presented as mean ± SEM. The single asterisk (*) indicates significant difference between baseline and postinfusion within a treatment with a $P < 0.05$; the double asterisk (**) indicates $P < 0.001$.

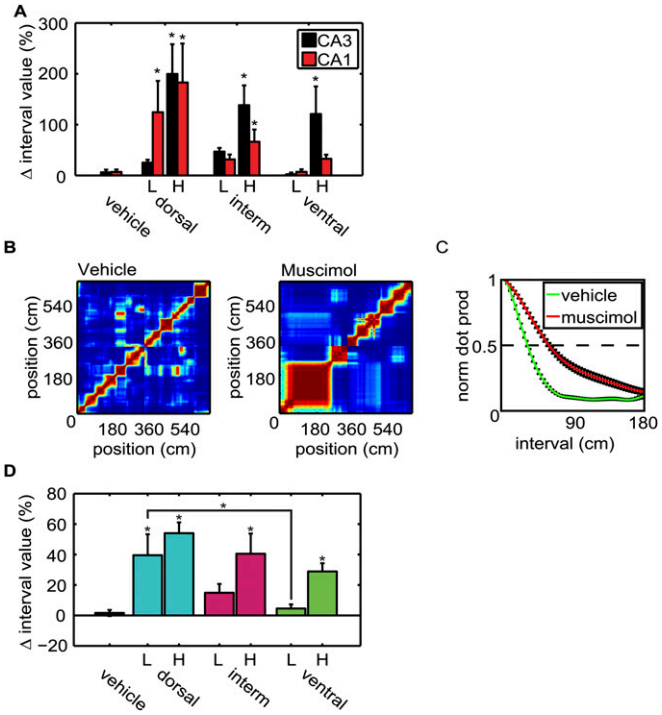

Fig. S4. Rate map population vector analysis and control. (*A*) Expansion of the spatial representation after focal MEC inactivation for CA3 and CA1. The mean change ± SEM in the interval value at which the correlation drops to 0.5 for all sessions. (*B*) Population vector cross-correlation matrices from vehicle and high-concentration muscimol trials for the same session as Fig. 3. The firing rates for the muscimol trial have been adjusted to control for decreased in-field rates and increased out-of-field rates. (*C*) The decorrelation curves for the two trials in *B* overlaid. The displayed data are the mean correlation ± SEM for each possible population vector pair interval between 0 and 180 cm. To quantify the scale of the spatial representation, the interval at which the correlation dropped to 0.5 was calculated (dotted line). (*D*) The mean change ± SEM in the interval value at which the correlation drops to 0.5 for all sessions using the adjusted rate maps for infusion trials. L indicates low concentration, and H indicates high concentration. Vehicle or site of inactivation is listed along the *Bottom*. The single asterisk (*) directly above error bars indicates significant difference from vehicle control calculated with post hoc test ($P < 0.05$). Bracket connecting individual bars indicates significant difference between effects of infusions at different infusion sites; the single asterisk (*) indicates $P < 0.05$.

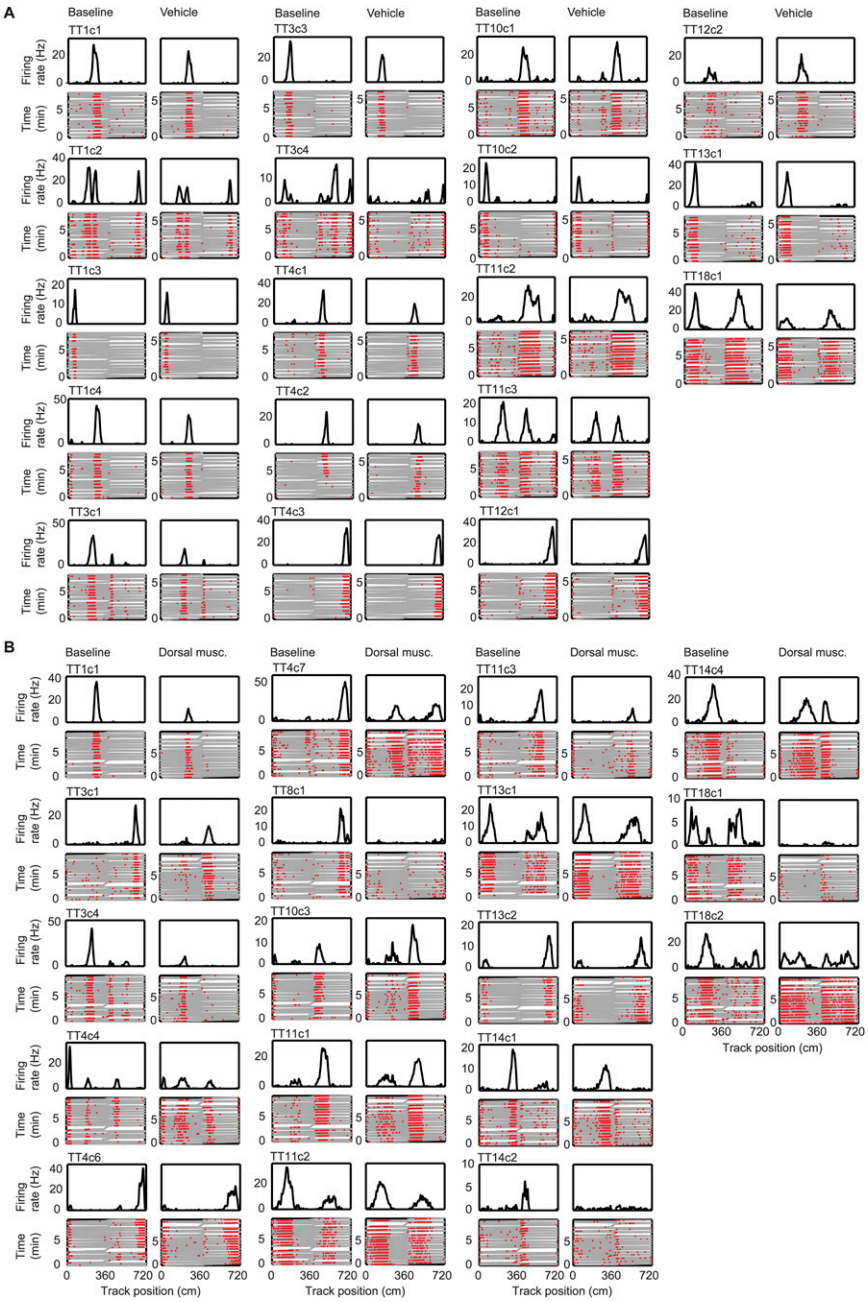

Fig. S5. Representative place cells. (*A*) Place cells from baseline and postvehicle infusion trials from a single session. (*B*) Place cells from baseline and post–high-concentration dorsal muscimol infusion trials from a single session. For each place cell, the top two panels are rate maps, and the bottom two panels denote individual spike position plotted against time on the track. Spikes are plotted in red, and path of the rat is plotted in gray.

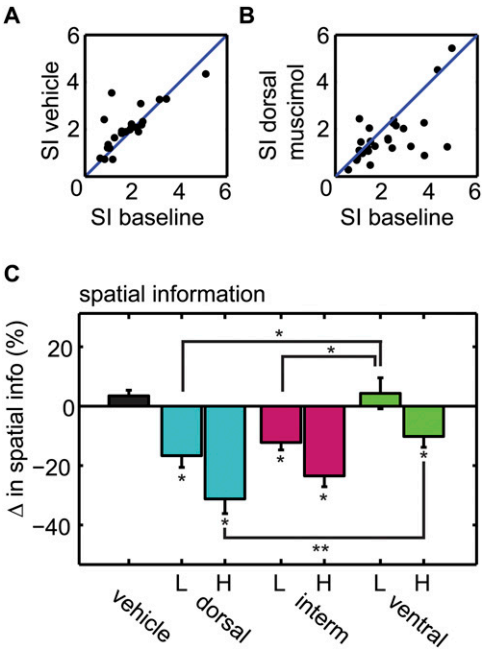

Fig. S6. Spatial Information. (*A*) Spatial information plot for place cells from before and after vehicle infusion. (*B*) Spatial information plot for place cells from before and after high-concentration dorsal infusion. For *A* and *B*, each place cell is plotted according to its spatial information score from the baseline trial on the *x* axis and its spatial information score from the infusion trial on the *y* axis. Note that most units have decreased spatial information scores after muscimol infusion. (*C*) The mean change ± SEM for all place cells combined across all tetrode bundles and CA3 and CA1 recording sites. L is for low concentration, and H is for high concentration. Vehicle or site of inactivation listed along the *Bottom*. The single asterisk (*) directly below error bars indicate significant difference from control ($P < 0.05$). Brackets connecting individual bars indicate a significant difference between the effects of infusions at different infusion sites; the single asterisk (*) indicates $P < 0.05$, and the double asterisk (**) indicates $P < 0.001$.

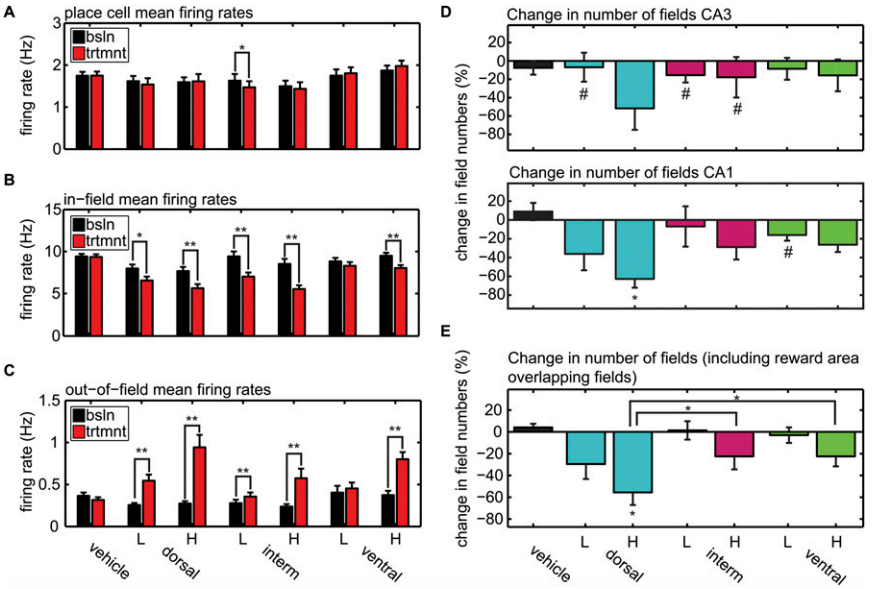

Fig. S7. Change in number of place fields. (*A*) Changes in place cell mean firing rates for all treatments. (*B*) Changes in place cell in-field mean firing rates for all treatments. (*C*) Changes in place cell out-of-field mean firing rates for all treatments. (*D*) Changes in the number of place fields for all treatments (*Top*, CA3; *Bottom*, CA1). (*E*) Changes in the number of place fields for all treatments combined across CA3 and CA1 recording sites and including fields that overlapped reward areas and/or other place fields. L is for low concentration, and H is for high concentration. Vehicle or site of inactivation is listed along the *Bottom*. Some subgroups had a low number of sessions; $n < 5$ is indicated by the number sign (#). The single asterisk (*) directly above or below error bar indicates significant difference from control with $P < 0.05$, and the double asterisk (**) indicates $P < 0.001$. Brackets connecting individual bars indicate a significant difference between the effects of infusions at different infusion sites; the single asterisk (*) indicates $P < 0.05$. L is for low concentration, and H is for high concentration. Vehicle or site of inactivation listed along the *Bottom*.

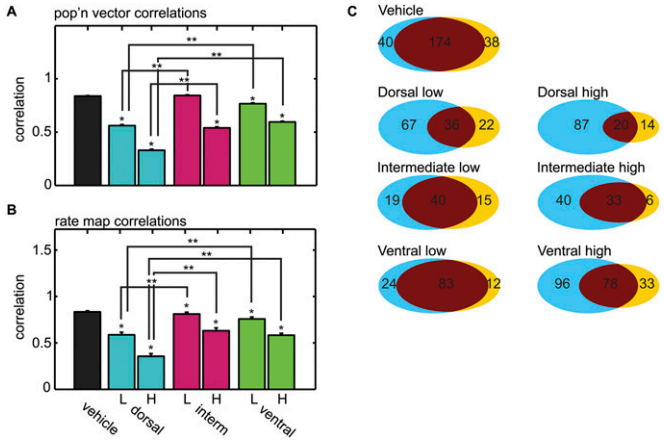

Fig. S8. Focal MEC inactivation induces remapping. (*A*) Mean ± SEM correlations between preinfusion and postinfusion population vectors; data grouped across CA3 and CA1 recording sites. (*B*) Mean ± SEM correlations between preinfusion and postinfusion individual unit rate maps; data grouped across CA3 and CA1 recording sites. L/H indicates low/high muscimol concentration. Vehicle or site of inactivation listed along the *Bottom*. The single asterisk (*) directly above error bars indicates significant difference between vehicle and corresponding treatment with a $P < 0.05$. Brackets connecting individual bars indicate significant differences between effects of infusions at different infusion sites; the double asterisk (**) indicates $P < 0.001$. (*C*) Venn diagrams of individual field numbers before and after infusion. Inner brown portions refer to the number of place fields from a given treatment group which were expressed during both preinfusion and postinfusion trials. Left-hand blue portions refer to the number of place fields expressed only during preinfusion baseline trials. Right-hand yellow portions refer to the number of place fields expressed only during postinfusion trials.

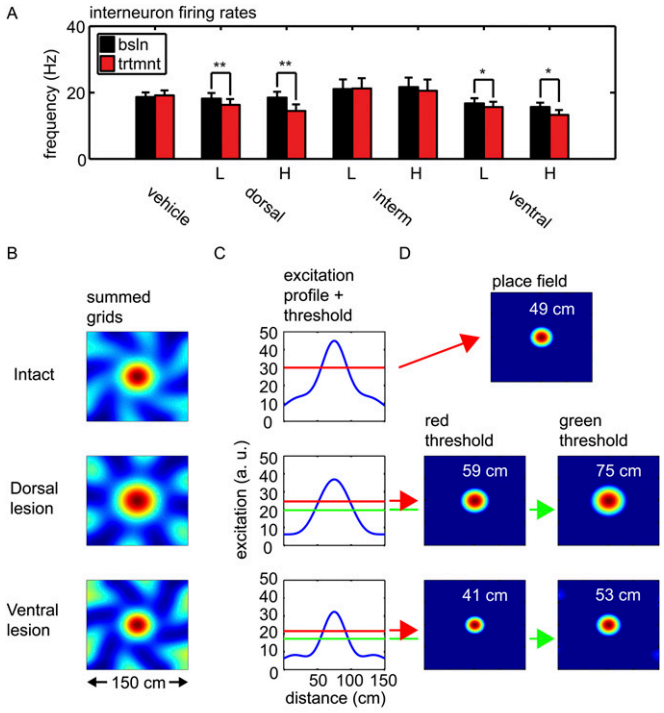

Fig. S9. Lesion/inactivation induced decreases in inhibition may contribute to place field expansion after loss of ventral grids. (*A*) Interneuron firing rates for all treatment subgroups (mean ± SEM). L denotes low-concentration muscimol, and H denotes high-concentration muscimol. Infusion sites are listed below. *$P < 0.05$, **$P < 0.001$. (*B*) Summation of six grid fields with internode spacing ranging from 40 to 231 cm (*Top*), four grid fields with spacing ranging from 80 to 231 cm (*Middle*), or four grid fields with spacing ranging from 40 to 115 cm (*Bottom*). (*C*) Firing-rate profiles (blue) for the summed grids in *B* taken from horizontal slices through center of the field. Threshold (red) is set to two-thirds of the peak excitation. Reduced threshold (green) is equal to 85% of red threshold. (*D*) Place fields resulting from applying the thresholds in *C* to the summed grid fields in *B*. The width of place fields (width of horizontal cross-section with firing rate over 1 Hz) in *Inset*.

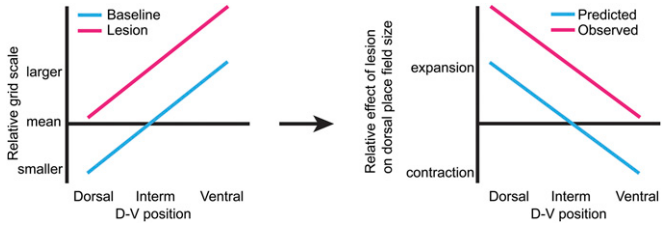

Fig. S10. Hypothetical effect of degradation of self-motion signal. Grid scale in spared portions of the MEC may increase after partial lesion or inactivation due to degradation of the self-motion signal, which causes the continuous attractor networks to move more slowly between adjacent states (*Left*). As a result of this secondary increase in grid scale following partial inactivation, lesion of ventral MEC does not produce the contraction of place fields predicted by the Fourier model, but rather produces a small amount of expansion (*Right*).

Table S1. Summary of predictions of the Fourier and self-motion gain change hypotheses

Prediction	Fourier	Gain change
Expansion of fields with dorsal inactivation	**Yes**	**Yes**
Expansion of fields with ventral inactivation	*No*	**Yes**
Contraction of fields with ventral inactivation	*Yes*	**No**
Increase in number of fields	Maybe	**No**
Decrease in number of fields	*No*	**Yes**
Substantial changes in field location	*No*	**Yes**
Change in precession slope	**Yes**	**Yes**
Change in intrinsic frequency	**Yes**	**Yes**
Increased "out-of-field" firing	**Yes**	*No*
Differential field change with dorsal and ventral MEC inactivations	**Yes**	Maybe
Differential field change with recording location along HPC dorsoventral axis	*Yes*	Maybe
Decrease in firing rate	Maybe	**Yes**

Predictions supported by the data are shown in bold. Those not supported are shown in italics. "Maybe" indicate no clear prediction by the hypothesis. HPC, hippocampus; MEC, medial entorhinal cortex.